INTERNATIONAL SYMPOSIUM on MUSICAL and ROOM ACOUSTICS
ISMRA 2016
September 11-13, 2016
La Plata, Buenos Aires, Argentina

Sound Production – Sound Synthesis:
Paper ISMRA2016-42

Bow control and playability of a two-polarisation time domain physical model of a bowed string

Charlotte Desvages [(a)], Michael Newton[(b)]

[(a)]Acoustics and Audio Group, University of Edinburgh, United Kingdom,
charlotte.desvages@ed.ac.uk
[(b)]Acoustics and Audio Group, University of Edinburgh, United Kingdom,
michael.newton@ed.ac.uk

Abstract

Many studies have explored bowed string control, first in theory, and later through experiments and simulations. Bowing control is most commonly described in terms of 3 parameters: downward bow force, bow position, and transverse bow velocity. The correlation between these parameters and the production of a note is generally referred to as the playability of the instrument. The musically-useful region within this parameter space where Helmholtz motion is achieved has been extensively researched. The coordination of these player-controlled parameters is crucial for the existence of steady-state oscillations, but also for their behaviour during note onset. Time domain models of bowed strings require the dynamic input of these physical control parameters. A detailed exploration of this parameter space is therefore of importance for playable physical models. In this work, a two-polarisation bowed string is coupled to a fully dynamic nonlinear lumped bow model. A finite difference scheme is used to solve the discretised equations of motion in the time domain. The bow-controlled input to the model is based on a two-dimensional force vector applied to the bow itself, coupling the two string polarisations. One force component is applied downwards, and the other orthogonally across the string axis, in contrast to the common convention of imposing a downward bow force and transverse bow velocity. The new model has the potential to allow for more realistic and dynamic gesture control. This study explores the parameter space implied by the model, relating it to the playability of the virtual instrument. Analysis of the steady state bow-string dynamics leads to classification of the playing regime, and a graphical representation inspired by the well known Schelleng diagram. The resulting playability-force diagrams may be used as an aid to control of the sound synthesis algorithm.

Keywords: bowed string synthesis, parameter mapping, virtual instrument control, Schelleng diagram, playing regime classification

INTERNATIONAL SYMPOSIUM on MUSICAL and ROOM ACOUSTICS
ISMRA 2016
September 11-13, 2016
La Plata, Buenos Aires, Argentina

Bow control and playability of a two-polarisation time domain physical model of a bowed string

1 Introduction

Bowed string playing is characterised by the high sensitivity of produced notes to small variations of bowing parameters. This allows an experienced player to have remarkable expressive control, whilst presenting the novice musician with significant challenges [1]. The ease with which a stable and desired note can be produced on a bowed string instrument is often referred to as the *playability* of the instrument [2]. This can be quantified by the breadth of the bowing parameter space that gives rise to Helmholtz motion [3] in the bowed string, which is characterised by a stick-slip cycle at the fundamental frequency of the string.

Numerous studies have investigated the playability of bowed strings, both experimentally [4, 5] as well as on virtual strings [6, 7]. Three control parameters have most frequently been used: the downwards/vertical bow force, transverse velocity, and bow-bridge distance. Schelleng [8] was the first to theorise analytical limits for the minimum and maximum bow downwards force, for given values of the two other parameters, outwith which Helmholtz motion is unattainable. He introduced a well-known graphical representation of the 'playable' region in the bowing parameter space, now commonly referred to as a 'Schelleng diagram'. Schelleng's analysis was recently revised by Schoonderwaldt et al. [9], who in particular found no clear dependence of the minimum bow force on bow velocity.

The control of physical modelling synthesisers remains a challenge. Models based on the behaviour of real instruments should exhibit both musically desirable and undesirable responses to user input, as seen in the physical objects they imitate. Evaluation and understanding of playability is therefore paramount for such synthesisers, particularly for virtual bowed strings.

In this work, a physical modelling algorithm of a string excited by a lumped, dynamic bow is presented. Three bow control parameters are employed, which each take the form of a time series: bow-bridge distance, downwards force, and transverse force exerted onto the bow. This is a departure from the usual bow-velocity control, and arises from the inclusion of an inertial, dynamic bow model. A modified graphical representation for playability is derived, adapted to this force-force control space, and based upon classification of the playing regime established after the initial transient phase. This is found to bear resemblance to the widely used force-velocity diagrams. Such a representation is potentially of use to players, who ultimately control all bow parameters during playing through the application of forces.

Section 2 describes the bowed string physical model and its numerical resolution. Section 3 outlines the approach taken for parameter exploration, and the method used to determine the playing regime achieved by the model in each case. Section 4 presents results of the analysis through graphical representations of the playable parameter space. Finally, Section 5 contextualises the results and discusses possible applications and improvements.

2 Two-polarisation bowed string model

The physical model used in this study is that of a simplified two-polarisation isolated linear string, simply supported at both ends, interacting with a lumped dynamic bow. The full model, numerical methods, and synthetic sound outputs are described in detail in a previous publication [10]. This section will briefly describe the key elements and control features of the model.

2.1 Model description

Consider an isolated, linear, stiff, lossy string, of length L (m), linear mass ρ (kg/m), tension T (N), bending stiffness B_s (N.m^2), damping coefficients λ_1 (1/s) and λ_2 (m^2/s). $w(x,t)$ and

$u(x,t)$ are the transverse displacement of the string in the directions, respectively, perpendicular (vertical polarisation) and parallel (horizontal polarisation) to the bow-string plane. They are functions of position $x \in [0,L]$ and time $t \in \mathbb{R}^+$.

This string is excited by a lumped bow of mass M_B (kg), at a fixed position x_B, reflected in the Dirac distribution $J_B = \delta(x - x_B)$; $w_B(t)$ and $u_B(t)$ are the position of the bow in the vertical and horizontal polarisations, respectively. The bow is subjected to external forces by the player in these two directions, respectively $f_{\text{ext},w}(t)$ and $f_{\text{ext},u}(t)$, and to linear losses in the horizontal polarisation, quantified by the coefficient λ_B (kg/s).

The equations describing the evolution of the string displacement and bow position are:

$$\mathscr{L} w = -J_B f_B \qquad \text{(1a)} \qquad\qquad M_B \ddot{w}_B = f_B + f_{\text{ext},w} \qquad \text{(1c)}$$

$$\mathscr{L} u = -J_B \left[f_B\right]_+ \varphi_B \qquad \text{(1b)} \qquad\qquad M_B \ddot{u}_B = -\lambda_B \dot{u}_B + \left[f_B\right]_+ \varphi_B + f_{\text{ext},u} \qquad \text{(1d)}$$

$$\mathscr{L} = \rho \partial_t^2 - T \partial_x^2 + B_s \partial_x^4 + \lambda_1 \rho \partial_t - \lambda_2 \rho \partial_t \partial_x^2 \qquad \text{(1e)}$$

where ∂_t, ∂_x are partial time and space derivation, respectively, and $[\cdot]_+ = \max(\cdot, 0)$. $f_B(\Delta_B)$ is the contact force exerted by the bow on the string, given by a penalty nonlinear damped collision model [11]:

$$f_B = \frac{\dot{\Phi}_B}{\dot{\Delta}_B} + \dot{\Delta}_B \Psi_B \qquad \Phi_B = \frac{K_B}{\alpha_B + 1} \left[\Delta_B\right]_+^{\alpha_B + 1} \qquad \Psi_B = K_B \beta_B \left[\Delta_B\right]_+^{\alpha_B} \qquad \Delta_B(t) = w(x_B, t) - w_B(t)$$

where $K_B > 0$, $\alpha_B > 1$ are collision coefficients related to the stiffness of the bow hair; $\beta_B > 0$ quantifies the nonlinear damping in the collision interaction.

The friction force exerted by the bow on the string is given by a friction coefficient $\varphi_B(v_{\text{rel}})$ depending on the relative velocity $v_{\text{rel}}(t) = \dot{u}(x_B, t) - \dot{u}_B(t)$ between the string and the bow, modulated by the normal bow force f_B. $\varphi_B(v_{\text{rel}})$ is given by [12]:

$$\begin{cases} |\varphi_B| \leqslant 1.2 & \text{if } v_{\text{rel}} = 0 \text{ (static)} \\ \varphi_B = \text{sign}(v_{\text{rel}}) \left(0.4 e^{\frac{-|v_{\text{rel}}|}{0.01}} + 0.45 e^{\frac{-|v_{\text{rel}}|}{0.1}} + 0.35\right) & \text{if } v_{\text{rel}} \neq 0 \text{ (kinetic)} \end{cases}$$

2.2 Discretisation and numerical resolution

The system (1) is discretised by the means of an implicit energy-balanced finite difference scheme [10], allowing the derivation of a recurrence equation in time. The state of the system is updated at an audio sample rate, computed from two preceding time steps.

Beyond the bow position along the string x_B (static during each simulation in the present study), the available dynamic control parameters are the forces exerted on the bow by the player in the two polarisations, $f_{\text{ext},w}(t)$ and $f_{\text{ext},u}(t)$ (discretised at audio sample rate into a pair of time series). The former will directly set the normal bow force, often referred to as 'bowing pressure' by musicians. The latter will dictate the transverse/horizontal bow velocity, through interaction with the string's friction characteristics.

Consequently, a bow force vector $\vec{f}_{\text{ext}}$ can be defined, whose orthogonal components are given by the normal/vertical and transverse/horizontal components of force, $f_{\text{ext},w}$ and $f_{\text{ext},u}$ respectively (see Figure 1). Such a description emphasises the role of the player in providing control through application of forces on the bow, from which all further quantities, such as bow velocity, and string dynamics, eventually arise.

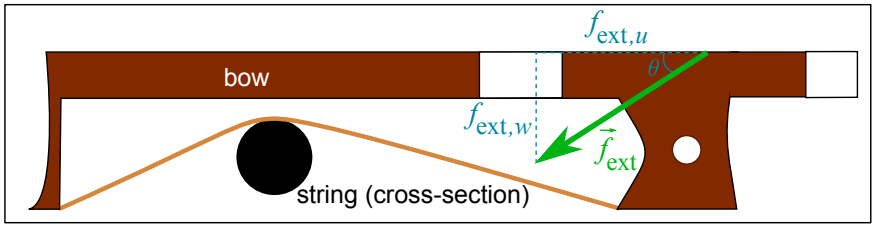

Figure 1: Bow control for this model is describable through the magnitude $\left|\vec{f}_{\text{ext}}\right|$ and angle θ of an external force vector acting on the bow.

3 Parameter exploration

3.1 Playability of a bowed string and graphical representation

The standard tool for playability analysis of bowed strings is the so-called Schelleng diagram [8], introduced as a two-dimensional logarithmic plot of the theoretical minimal and maximal bow force limits versus bow-bridge distance, for a given bow velocity. Each of these limits form a straight line in this logarithmic parameter space, delimiting a triangular area within which Helmholtz motion is attained. Beyond these limits, other vibration states arise, such as:

- Raucous motion, when the downwards bow force is high for a given transverse bow velocity and bow-bridge distance, preventing the string from detaching from the bow at the end of the sticking phase, and giving rise to a rough, noisy sound.
- Multiple slipping, when the downwards bow force is too low for a given transverse bow velocity and bow-bridge distance, preventing the bow from sticking to the string for the entirety of the nominal sticking phase, and often characterised by strong even harmonics in the produced note, as the string slips several times per nominal period.
- Anomalous low frequencies (ALF), beyond the maximal downwards bow force limit, when the Helmholtz corner is reflected once or more between the bow and nut before triggering slipping, resulting in oscillations at, typically, integer multiples (or slightly less) of the nominal period; the so-called secondary waves (ripples) reflecting between the bow and bridge could also yield another type of ALF, with a shorter period lengthening, correlated to the bow-bridge distance [13].
- S-motion, observed for high downwards bow forces and bow-bridge distances, characterised by high-amplitude ripples [14].

3.2 An alternative approach: playability-force diagrams

The main difference between the control of classic bowed string models, and the model presented here, is the transverse bow control. The conventional control parameter is the 'imposed' transverse bow velocity. The present model, however, uses a time series describing the force applied to the bow. As noted in Figure 1, the bow parameters that give rise to steady Helmholtz motion, or any other playing regime, can therefore be described in terms of the magnitude and angle of this bow force vector.

In his study of steady-state oscillations, Schelleng [8] chose a particular representation of the parameter space and bow force limits, as a function of the bow-bridge distance, for a given bow velocity. However, as noted in his original work, one could also plot the vertical bow force as a function of the bow velocity, for a given bow-bridge distance. An obvious layout for visualising the parameter space in the present framework immediately arises: the bow force vector can be represented in a playability diagram, with its transverse component $f_{\text{ext},u}$ on the horizontal axis and normal component $f_{\text{ext},w}$ on the vertical axis, and with the origin of the graph (chosen to lie at the top right of the axes) corresponding to the origin of $\vec{f}_{\text{ext}}$ (i.e. application of zero force). An

example of this 'playability-force diagram' is shown in Figure 2. In terms of conventional bow force limits, the apex of the bow force vector might be expected to navigate a two-dimensional valley in the bow force parameter space, within which steady Helmholtz motion is possible.

3.3 Generating the simulated data

A large number of simulations were run using the algorithm described in Section 2.2. Ten data sets were obtained, for ten static bow positions x_B, determined relative to the string length. The ten positions were chosen as integer ratios, x_B^{int}, of the string length, for x_B^{int} values from 5 to 14, so that the bow was positioned at $1/x_B^{int}$ of the string length away from the bridge.

For each of the ten positions, the downwards bow force $f_{\mathrm{ext},w}$ was incrementally varied from 0.02 to 3 N in 0.02 N steps (150 different force values), and the transverse bow force $f_{\mathrm{ext},u}$ was varied between 0.05 and 6 N in 0.05 N steps (120 different force values), amounting to 18000 simulations per bow position. Each simulation lasted for 3 seconds, with the downwards bow force applied at $t = 0$, and the transverse bow force ramped up to its target value at $t = 1$ s. This delay allowed any initial string oscillations, caused by the application of the downwards bow force, time to settle. The playing regime classification routine examined the simulation output from 1.8s after application of the transverse bow force, i.e. well after the starting transient.

3.4 Steady-state classification

Automatic classification of bowed string playing regimes has been attempted numerous times [2, 15, 16, 17, 18]. The approach taken varies according to the data available. For experimental measurements, it is not usually possible to have direct information about the stick/slip behaviour at the point of bow-string contact (i.e. the actual relative velocity of the bow-string coupling point). Rather, analysis must be based upon time histories of the string velocity, or, most commonly, through a measurement of the force applied by the string to the bridge, through use of an accelerometer or vibrometry system. In the simulated world, however, it is straightforward to obtain the relative bow-string velocity at the bowing point, so providing direct information about the bow-string dynamics. The present classification routine is based entirely upon analysis of this relative bow-string velocity signal, $v_{\mathrm{rel}}(t)$, obtained from the simulations.

The approach uses autocorrelation to identify periodicity, and is broadly in line with the methodology outlined by Woodhouse [17], with one notable difference. Rather than applying an autocorrelation analysis directly to v_{rel}, a peak-finding algorithm is first applied to v_{rel} to identify moments of maximal 'slip' within the stick/slip cycle. The timing and amplitude of these peaks are used to create a 'quantised' version of v_{rel}, called v_{rel}^q, that consists of zeros everywhere except at moments of maximal slip, where v_{rel}^q has a value equal to the maximal slip amplitude.

Autocorrelation analysis is applied to the quantised relative bow-string velocity v_{rel}^q, over a window of 40ms, beginning 1.8s after application of the horizontal bow force. This window covers several cycles of the anticipated fundamental period of the string. Autocorrelation of this quantised signal produces an autocorrelation function (ACF) that is itself of a quantised nature, with broad regions of zero-amplitude, interspersed with correlation peaks. Analysis of the location, spacing and spread of these peaks led to a number of relatively simple rules/checks allowing classification of each simulation run into one of six categories: constant slipping (where the bow slides smoothly over the string, with no clear stick/slip cycle), constant sticking (where the transverse force is too small to keep the bow moving, the bow stops and remains permanently stuck to the string), Helmholtz motion, multiple slipping motion, anomalous low frequencies (ALF), and raucous behaviour. The detection of S-motion was not included in this study.

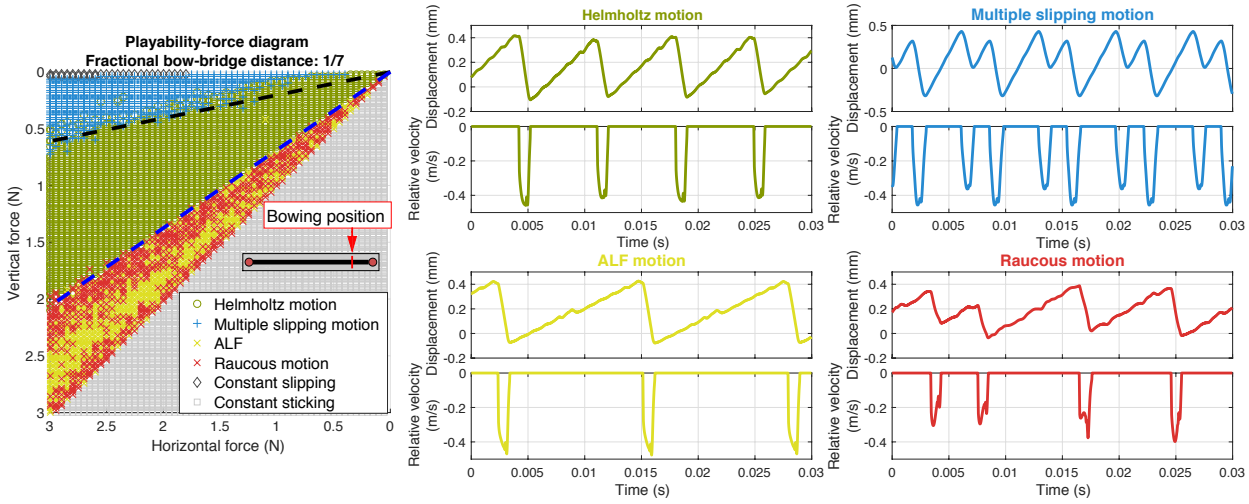

Figure 2: An example playability-force diagram. Each simulation was examined 1.8s after initial application of the horizontal bow force, and categorised into one of six playing regimes. Typical string displacement and associated relative velocity waveforms are shown for each of the four detected stick-slip regimes. The diagonal black and blue lines on the diagram mark the estimated minimum and maximum bow force angles, respectively, between which Helmholtz motion is reliably obtained from the simulation, regardless of bow force magnitude.

4 Results

4.1 Bow force vector range and areas of interest

The playability-force diagrams mostly appear divided into approximately triangular regions. The Helmholtz-playable region (Figure 2, in green) is circumscribed by two limits. Below, there is an almost linear separation, corresponding to a particular angle of the bow force vector, between Helmholtz motion and raucous behaviour (in red). Careful listening of simulations on either side of this division suggests the classification algorithm is robust. Above the Helmholtz region, the transition into the multiple slipping region is generally less distinct, especially for very low/high bow force vector magnitudes (i.e. close to, or far away from, the origin). This suggests a more ambiguous transition between Helmholtz motion and multiple slipping at low downwards forces. Within the raucous area, one or more triangular-shaped ALF areas (in yellow) appear for all values of x_B.

The clearly defined, and apparently linear, maximum downwards bow force limit, within the analysis framework used here, suggests a possible definition of the lower limit of the playable space in terms of the bow force vector angle only, independently of its magnitude. With the aim of clarifying the playability of the model as a sound synthesis tool, a 'soft' upper limit can similarly be drawn from the origin, bounding an angle range where Helmholtz motion is reliably achieved regardless of bow force magnitude, and excluding all occurrences of multiple slipping. Figure 2 shows these upper (in black) and lower (in blue) limits.

4.2 Evolution of the playable range with bow position

Figure 5 presents all ten playability-force diagrams, for fractional bow-bridge distances from $\frac{1}{5}$ to $\frac{1}{14}$ of the length of the string. All regions of the diagram seem to rotate counter-clockwise around the origin as the bow gets closer to the bridge. Both lower and upper downwards bow force limits shift towards higher values. The raucous/ALF section narrows, as the multiple slipping area expands, confirming the need for higher downwards forces to trigger Helmholtz motion as the bow-bridge distance decreases. The lower downwards bow force limit, separating multiple slipping and Helmholtz regimes, appears increasingly linear as the string is bowed nearer the bridge. Within the multiple slipping region, various 'pockets' of Helmholtz motion are

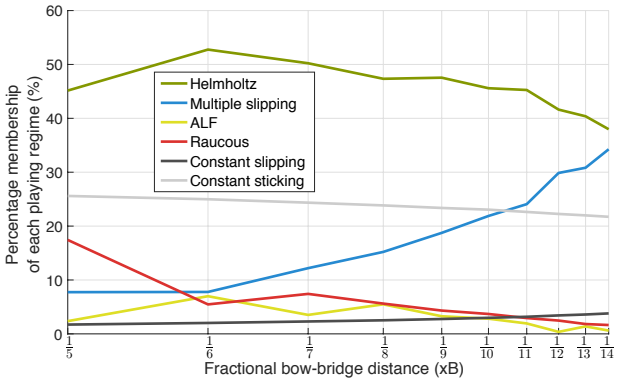

Figure 3: Relative membership counts for detected playing regimes for varying bow position.

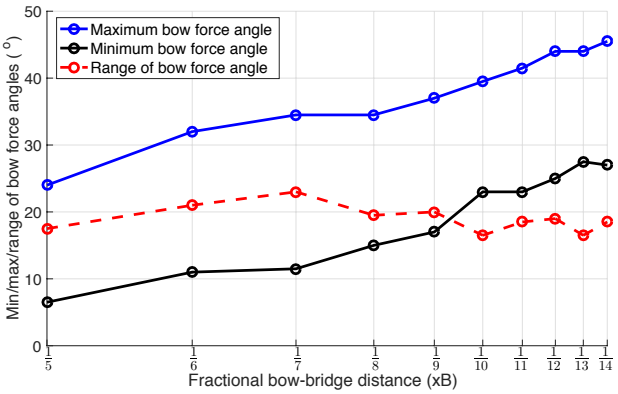

Figure 4: Estimated minimum, maximum and implied range of bow force angles that produce reliable Helmholtz motion, vs. bow position.

seen to appear, change size, and rotate anti-clockwise with decreasing bow-bridge distance.

To get a better sense of how playability might evolve with decreasing bow-bridge distance, and to relate the behaviour of this model to a more conventional Schelleng analysis, two quantities are plotted against bow position. Figure 3 shows the evolution of the relative area of each detected regime versus bow position, by counting, for each bow-bridge distance, the number of cases belonging to a particular category. The result summarises one of the most obvious trends seen across the playability-force diagrams, which is the progressive rise in cases of multiple slipping with decreasing bow-bridge distance. Furthermore, beyond a peak in x_B of $\frac{1}{6}$, the Helmholtz region gradually shrinks.

Figure 4 shows the variation of the angular range of the bow force vector giving reliable Helmholtz motion, with decreasing bow-bridge distance. This is evaluated by measuring the respective angles of the dark blue and black lines used to delimit a reliable Helmholtz-playable range independently of the bow force magnitude (see Figure 2), as described in Section 4.1. While the minimum and maximum bow angles both increase with decreasing bow-bridge distance, the playable angle range does not seem to follow a clear and systematic trend. Indeed, the variations in playable range cover just a few degrees, which is close to the uncertainty in the assignment of the upper line, bounding the Helmholtz and multiple slipping regions. Further work is required to explore and quantify the characteristics of this upper transition zone.

4.3 Anomalous low frequencies

An ALF band (in yellow) seems to appear on all diagrams, suggesting a 'playable ALF region' rather than random, sparsely located cases, in line with previous findings [9]. This ALF region moves around the raucous region with varying bow position, surrounded by raucous cases further from the bridge, and shifting progressively in an anti-clockwise direction towards the bridge. Eventually it provides a clear separation between raucous cases at lower vertical bow forces, and constant sticking at higher vertical bow forces (e.g. for x_B from $\frac{1}{8}$ to $\frac{1}{14}$).

For $x_B = \frac{1}{5}$ (Figure 5, top left), two triangular bands can be observed within the raucous triangle. One of them, in yellow, corresponds to the first type of ALF described in Section 3.1, where the fundamental period is almost doubled. The second one, in green, was automatically classified as Helmholtz motion, as the classification algorithm tolerates a moderate amount of pitch flattening. However, closer inspection of the waveforms shows what could be the second described type of ALF, due to ripples reflecting between the bridge and bow, where the pitch is lowered by about one semitone. Without further analysis, this second band becomes undistinguishable from pitch-flattened Helmholtz motion for smaller bow-bridge distances.

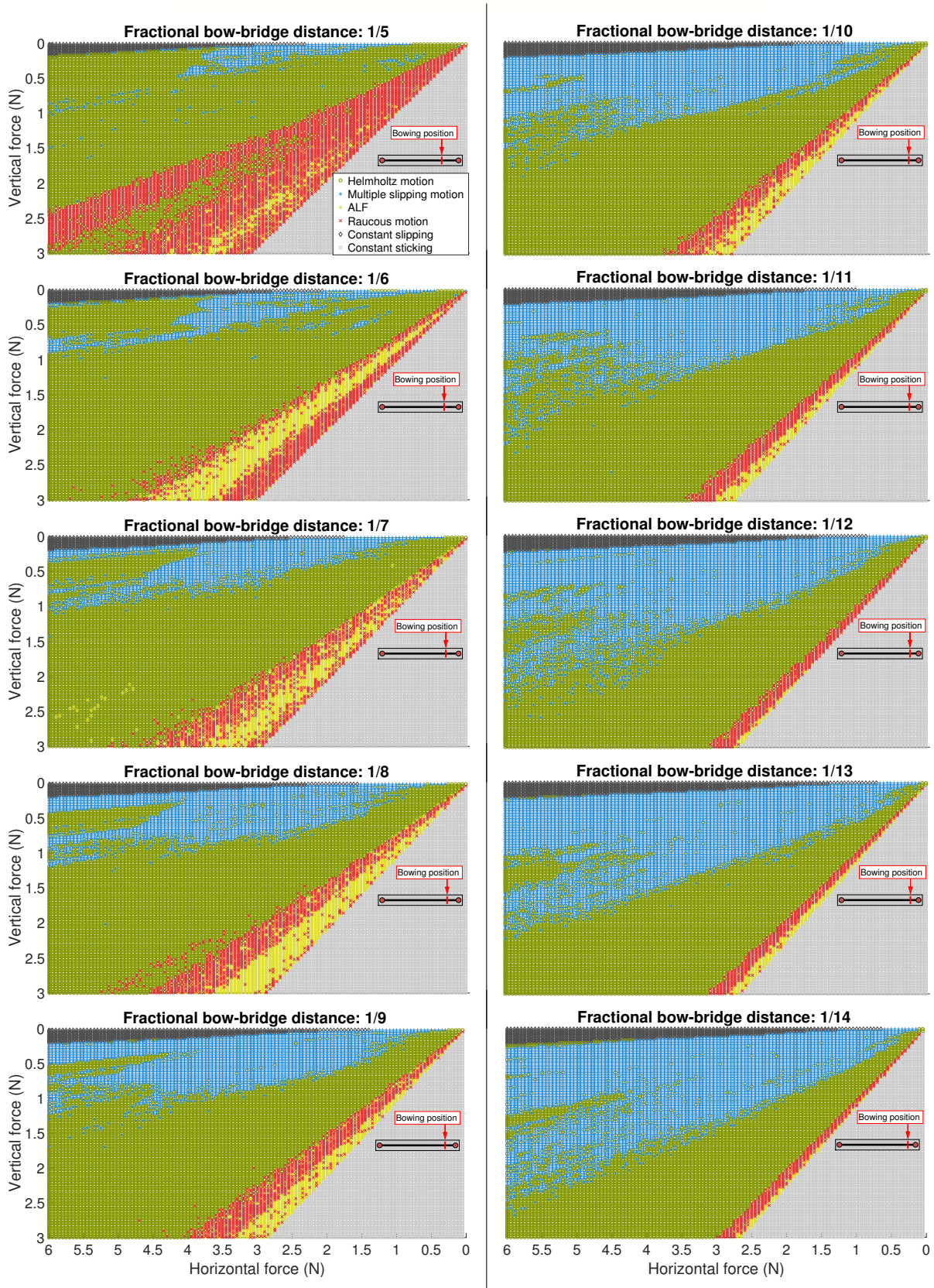

Figure 5: A series of playability-force diagrams, each evaluated over the same range of bow force vector magnitudes and angles. The axes have been adjusted so that zero force is at the top-right of each plot. Components of increasing vertical and horizontal bow force are directed towards the lower left corner, as per Figure 1. Note that rotation of the bow itself is not implied.

5 Discussion

This paper presents a physical model of a bowed string, where the bow is driven by a force vector with a downwards and a transverse component. The numerical methods for solving the partial differential equations describing the bow-string system allow for the simulation of the full string displacement, as well as the inclusion of important nonlinear effects. However, the sound synthesis algorithm is difficult to control intuitively. This study provides an initial exploration of the range of bowing parameters giving rise to various steady-state oscillation regimes in the simulated bowed string. A tool is developed in order to visualise the playable space of this particular model, through a systematic regime classification, producing a playability-force diagram inspired by the widely used Schelleng diagrams.

The resulting plots indeed show some similarities with Schelleng diagrams, in that a triangular Helmholtz-playable area can be observed, in terms of downwards and transverse bow force components. This area is bounded below (high downwards force) by a clear zone of raucous and ALF behaviour, and above (low downwards force) by a less clearly delimited multiple slipping zone. The less defined transition between the Helmholtz and multiple slipping region could result from the progressive character of the transition between Helmholtz motion and multiple slipping, as observed in [9]. Many of the cases shown in Figure 5 that lie on the edge of the Helmholtz/multiple slipping region, and even clearly beyond, exhibited clear transitions between Helmholtz and multiple slipping behaviours over the course of 2s of simulation time. Analysis based upon the string behaviour after 1.8s of run time is clearly a somewhat arbitrary choice, especially for these cases. Re-analysis of the whole dataset based upon a different analysis window would certainly produce a different set of playability-force diagrams. Indeed, it seems logical to extend the present work to examine the transient characteristic, along the lines of Guettler and Askenfelt [19], the subtle evolution of which is certainly vital in determining the later steady/transitionary playing regime.

The results of the proposed analysis are first and foremost intended to be used as a tool for guiding sound synthesis with the bow-force-controlled physical modelling algorithm. Before any comparison can be made with real bowed strings, it must be considered that the physical model used for this study is missing some arguably essential features, potentially having great influence on playability, e.g. a finite bow width, a better calibration of the damping coefficients to match the string loss profile in the frequency domain, and perhaps most importantly, a mobile bridge boundary, coupled to a realistic bridge-body model. The influence of torsional waves, not considered here, on playability, has been studied on real [20] and virtual [6] bowed strings.

The analysis of minimum and maximum limits to determine the playable range of the bow force angle is acknowledged as requiring further refinement, but is nevertheless an interesting result for the physical model employed. A regression analysis could help to more accurately measure the evolution of the bow force limits bounding the Helmholtz range with varying bow position, further clarifying the observations of Section 4.2.

This exploratory study is a first step to several applications and extensions. First, in terms of sound synthesis, a database of compiled diagrams for a range of strings with known physical parameters could be stored, and used as part of a collection of presets for the sound synthesis of particular strings. The scale, resolution, and repeatability of the simulations could also allow exploration of the influence of a particular parameter or bowed string feature on the size and shape of the Helmholtz-playable space.

An advantage of the force vector representation is that the same bowing parameters, and therefore the same existing data sets, can be used for transient analysis. Indeed, while a constant transverse bow force $f_{\mathrm{ext},u}$ results in a constant bow velocity (due to damping terms), a step onset of such a force is arguably comparable to the application of an initial transverse

acceleration to the bow, which is the control used for transient analysis by Guettler [21]. A similar diagram to that used for steady-state analysis can now be drawn, to explore the range of initial bow force angles and magnitudes yielding an 'acceptable' transient [19].

Acknowledgements

This work was supported by the Edinburgh College of Art, the Audio Engineering Society Educational Foundation, and the European Research Council under grant number ERC-2011-StG-279068-NESS.

References

[1] J. Woodhouse, "Playability of bowed-string instruments," in *Proc. Stockholm Mus. Acoust. Conf.*, Stockholm, Sweden, 2013, pp. 3–8.

[2] P. M. Galluzzo, "On the playability of stringed instruments," Ph.D. dissertation, Trinity College, Dublin, 2004.

[3] H. von Helmholtz, *On the sensations of tone as a physiological basis for the theory of music (English translation A.J. Ellis, 1885, 1954); third edition*. Cambridge, UK: Cambridge University Press, 2009.

[4] C. Raman, "On the mechanical theory of the vibrations of bowed strings and of musical instruments of the violin family, with experimental verification of the results," *Bulletin of the Indian Association for the Cultivation of Science*, vol. 15, pp. 1–158, 1918.

[5] A. Askenfelt, "Measurement of the bowing parameters in violin playing. II: Bow-bridge distance, dynamic range, and limits of bow force," *J. Acoust. Soc. Am.*, vol. 86, no. 2, pp. 503–516, 1989.

[6] S. Serafin, J. O. Smith III, and J. Woodhouse, "An investigation of the impact of torsion waves and friction characteristics on the playability of virtual bowed strings," in *Proc. IEEE Workshop Appl. Signal Process. Audio Acoust.*, New Paltz, New York, 1999, pp. 1–4.

[7] D. Young and S. Serafin, "Playability evaluation of a virtual bowed string instrument," in *Proc. Conf. New Interf. Mus. Expr.*, Montreal, Canada, 2003, pp. 104–108.

[8] J. C. Schelleng, "The bowed string and the player," *J. Acoust. Soc. Am.*, vol. 53, no. 1, pp. 26–41, 1973.

[9] E. Schoonderwaldt, K. Guettler, and A. Askenfelt, "An empirical investigation of bow-force limits in the Schelleng diagram," *Acta Acust. united Ac.*, vol. 94, no. 4, pp. 604–622, Jul. 2008.

[10] C. Desvages and S. Bilbao, "Two-polarisation physical model of bowed strings with nonlinear contact and friction forces, and application to gesture-based sound synthesis," *Appl. Sci.*, vol. 6, no. 5, p. 135, 2016.

[11] K. H. Hunt and F. R. E. Crossley, "Coefficient of restitution interpreted as damping in vibroimpact," *J. Appl. Mech.*, vol. 42, no. 2, pp. 440–445, 1975.

[12] J. H. Smith and J. Woodhouse, "The tribology of rosin," *J. Mech. Phys. Solids*, vol. 48, pp. 1633–1681, 2000.

[13] E. Schoonderwaldt, "The violinist's sound palette: spectral centroid, pitch flattening and anomalous low frequencies," *Acta Acust. united Ac.*, vol. 95, no. 5, pp. 901–914, Sep. 2009.

[14] B. Lawergren, "On the motion of bowed violin strings," *J. Acoust. Soc. Am.*, vol. 44, no. 3, pp. 194–206(13), Mar. 1980.

[15] R. T. Schumacher and J. Woodhouse, "The transient behaviour of models of bowed-string motion." *Chaos (Woodbury, N.Y.)*, vol. 5, no. 3, pp. 509–523, 1995.

[16] P. M. Galluzzo and J. Woodhouse, "High-performance bowing machine tests of bowed-string transients," *Acta Acust. united Ac.*, vol. 100, no. 1, pp. 139–153, Jan. 2014.

[17] J. Woodhouse, "Bowed string simulation using a thermal friction model," *Acta Acust. united Ac.*, vol. 89, no. 2, pp. 355–368, 2003.

[18] H. Mansour, J. Woodhouse, and G. Scavone, "Time-domain simulation of the bowed cello string: Dual-polarization effect," in *Proc. Meet. Acoust.*, vol. 19, Montreal, Canada, 2013, p. 035014.

[19] K. Guettler and A. Askenfelt, "Acceptance limits for the duration of pre-Helmholtz transients," *J. Acoust. Soc. Am.*, vol. 101, no. 5, pp. 2903–2913, 1997.

[20] E. Bavu, J. Smith, and J. Wolfe, "Torsional waves in a bowed string," *Acta Acust. united Ac.*, vol. 91, no. 2, pp. 241–246, 2005.

[21] K. Guettler, "On the creation of the Helmholtz motion in bowed strings," *Acta Acust. united Ac.*, vol. 88, pp. 970–985, 2002.